

DOI: 10.13476/j.cnki.nsbdkq.2021.0061

刘超凡, 夏伟, 王继保, 等. 向家坝水电站过机泥沙的多重分形特性[J]. 南水北调与水利科技(中英文), 2021, 19(3): 581-589.  
LIU C F, XIA W, WANG J B, et al. Multifractal characteristics of sediment pass by the Xiangjiaba Hydropower Station[J].  
South-to-North Water Transfers and Water Science & Technology, 2021, 19(3): 581-589. (in Chinese)

# 向家坝水电站过机泥沙的多重分形特性

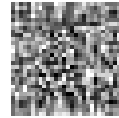
刘超凡<sup>1</sup>, 夏伟<sup>1</sup>, 王继保<sup>1</sup>, 许学问<sup>2</sup>, 陈和春<sup>1</sup>, 陈艳超<sup>1</sup>

(1. 三峡大学水利与环境学院, 湖北 宜昌 443002; 2. 湖北省水利水电规划勘测设计院, 武汉 430064)

**摘要:**以向家坝水电站过机泥沙为研究对象,采用激光粒度仪分析过机泥沙粒径级配的体积百分比,运用多重分形理论对粒径分布的特征规律进行研究。结果表明:过机泥沙粒径具有良好的多重分形特性,结合多重分形理论,粒径分布整体平均上的不均匀大小为  $D_1(B_2) > D_1(C_1) > D_1(C_2) > D_1(A_2) > D_1(B_1) > D_1(A_1) > D_1(D_2) > D_1(D_1)$ ; 存在某一阈值  $q$ ,使得当  $q \geq 5$  时,最大子集粒径分布的不均匀大小为  $D \geq 5(B_2) > D \geq 5(B_1) > D \geq 5(D_2) > D \geq 5(C_2) > D \geq 5(A_2) > D \geq 5(C_1) > D \geq 5(A_1) > D \geq 5(D_1)$ ,当  $q \leq -7$  时,最小子集粒径分布的不均匀大小为  $D \leq -7(C_1) > D \leq -7(B_2) > D \leq -7(A_1) > D \leq -7(D_1) > D \leq -7(C_2) > D \leq -7(A_2) > D \leq -7(D_2) > D \leq -7(B_1)$ (其中  $A_1$ 、 $B_1$ 、 $C_1$ 、 $D_1$  为左岸机组过机泥沙样品编号,  $A_2$ 、 $B_2$ 、 $C_2$ 、 $D_2$  为右岸机组过机泥沙样品编号);多重分形奇异谱谱宽  $\Delta\alpha$  应分为最小子集和最大子集奇异谱谱宽  $\Delta\alpha_1$  和  $\Delta\alpha_2$  分别计算;结合广义维数谱和多重分形奇异谱,关于粒径分布在局部上的不均匀程度,两者的结论是相同的;结合相关性分析,泥沙细化和最大子集分布不均匀大小呈现良好的负相关性,而泥沙细化和最小子集分布不均匀大小无关。

**关键词:**水电站;过机泥沙;多重分形理论;粒径分布

中图分类号:TV145 文献标志码:A 开放科学(资源服务)标志码(OSID):



水电站发电效益与水轮机磨蚀问题长期困扰着水利工程师,尤其是汛期暴雨高发季节,入库流量和泥沙含量均达到了峰值,此时水电站发电效益最佳,而水轮机过流部件磨蚀也最严重。大多数水电站修建在高山峡谷地区,水流挟带着大量泥沙,使得水轮机不可避免地会面临磨蚀问题,尤其是洪水暴雨频发的夏季。水轮机过流部件内水流速度大、过机泥沙含量高,使得磨蚀问题更加突出。研究<sup>[1]</sup>表明,河流泥沙是从流域地表侵蚀冲刷而来,主要受降雨驱动。在降雨作用下,雨滴击溅和径流冲刷破坏土壤结构,使土壤颗粒发生分离、搬运,随径流汇入河流,这一过程受暴雨作用显著<sup>[2]</sup>。过机泥沙粒径分析是研究水轮机过流部件磨蚀必不可少的参数。泥沙粒径级配反映了泥沙颗粒各级粒径的百分含量情况,是进行泥沙研究的基础资料:(1)分析泥沙粒径与单

重分形或絮凝的相关性<sup>[3-6]</sup>; (2)通过分析泥沙特征粒径(中值粒径、平均粒径)的时空变化规律来研究流域泥沙细化趋势<sup>[7-8]</sup>; (3)为河床演变、泥沙起动规律、水流挟沙力和水轮机磨蚀等提供基础资料分析<sup>[9-12]</sup>。泥沙粒径是河流泥沙的重要几何特征,泥沙特征粒径是泥沙颗粒统计平均的概括,但泥沙颗粒级配尚不足以完全反映其不均匀性,也无法显示出泥沙的均匀程度和细节。分形理论的创立和应用打破了传统通过泥沙各粒径级配颗粒含量表征泥沙粒径分布的方式,为定量描述泥沙粒径分布提供了新途径<sup>[13]</sup>。分形维数可以定量地表征颗粒粒径分布的奇异性和自相似性,并反映其复杂程度。颗粒粒径分形研究始于1995年,Perfect等<sup>[14]</sup>利用单重分形理论定量研究了土壤颗粒粒径的分形特征,随后分形理论广泛应用于颗粒分布研究中,取得了大

收稿日期:2020-02-21 修回日期:2020-06-10 网络出版时间:2020-06-19

网络出版地址:https://kns.cnki.net/kcms/detail/13.1430.TV.20200619.1427.004.html

作者简介:刘超凡(1996—),女,湖北宜昌人,主要从事水工模型试验、河流动力学研究。E-mail:724750639@qq.com

通信作者:王继保(1976—),男,湖北宜昌人,副教授,主要从事水工模型试验、河流动力学研究。E-mail:435744600@qq.com

量成果<sup>[15-17]</sup>。在此基础上,Grout 等<sup>[18]</sup>指出自然系统中泥沙粒径分布绝大部分符合多重分形原则,利用多重分形方法可以更为准确地分形颗粒粒径分布特征。此后,多重分形理论在颗粒分布研究中得到了广泛应用<sup>[19-21]</sup>。

目前,关于颗粒粒径分布的多重分形研究主要集中在土壤粒径分布领域,对于过机泥沙粒径的多重分形分析尚无相关研究进展。为此,选取向家坝水电站过机泥沙为研究对象,基于激光粒度仪精确测量的过机泥沙粒径级配资料,引入多重分形理论,结合多重分形的广义维数谱和多重分形奇异谱函数来定量探究过机泥沙粒径在时间尺度上的变异性和不均匀程度,为过机泥沙粒径分布研究提供一种新思路。

向家坝水电站位于金沙江下游段,设左岸坝后厂房和右岸地下厂房,共安装 8 台单机容量 800 MW 水轮发电机组,建成后发挥着巨大的防洪和发电效益。作为电站核心设备的水轮机,其性能的好坏和运行的可靠性是能否发挥工程效益的关键所在之一。而金沙江下游具有河床陡峻,水流挟沙能力强,降水量年内分布不均,主要集中在汛期 7—10 月,输沙量高度集中在汛期的特点。为及时了解泥沙对水轮机的破坏规律,研究减缓含沙水流对水轮机过流部件表面的磨蚀破坏的各项防护措施,需要开展向家坝水电站左右岸典型机组的过机泥沙的中长期检测,并为后续水轮机防护措施的开发提供数据支撑。

## 1 研究方法

### 1.1 工程背景

向家坝水电站位于四川宜宾市和云南省水富县交界处,下距水富县仅 1.5 km,距宜宾市约 33 km,是金沙江流域下游梯级电站开发中的最末一级,坝址控制流域面积约 45.88 万 km<sup>2</sup>,占金沙江流域面积的 97%。金沙江流域中下游段高山峡谷纵横、河段狭窄、水流湍急、流态复杂,也是流域泥沙主要来源地,多年平均含沙量 1.7 kg/m<sup>3</sup>,约为三峡入库沙量的 1/2。向家坝水电站建成后,金沙江输沙量高度集中在汛期的特性,合理调度可使大部分入库泥沙淤积在死库容内,在不影响发电效益的同时能够有效拦截流域泥沙进入下游的三峡库区。

### 1.2 采样及研究方法

以向家坝水电站为背景,汛期 6—9 月过机泥沙为研究对象,考虑到汛期过机泥沙粒径分布在时间上的差异性,每月选择两次最大泥沙含量的过机泥沙进行采样。每次采样时,选取左岸和右岸典型机组,进

入指定的水轮机蜗壳内部取水口进行水样采集。整个汛期共采样 8 次,共 8 个样品,在过机含沙水流采样现场取样后,将样品带回实验室,根据取样水体中含沙量对水样进行 1~2 周的沉淀,然后提取。按采样时间顺序依次编号为左岸机组过机泥沙样品 A<sub>1</sub>、B<sub>1</sub>、C<sub>1</sub>、D<sub>1</sub> 和右岸机组过机泥沙样品 A<sub>2</sub>、B<sub>2</sub>、C<sub>2</sub>、D<sub>2</sub>。

河流泥沙是从流域侵蚀冲刷而来的,主要受降雨驱动。河流泥沙也是土壤颗粒在河流中的一种存在状态,其多重分形参数计算可以参考土壤颗粒的多重分形参数计算。一般土壤颗粒粒径的测量区间选为 0.02~2 000 μm,河流泥沙来源于流域地表土壤颗粒,但河流泥沙粒径分布又区别于土壤颗粒粒径分布,其一方面受降雨驱动下侵蚀泥沙颗粒分选及搬运机制的影响<sup>[22]</sup>,另一方面受泥沙起动沉积规律的影响<sup>[23]</sup>,表现在粗颗粒泥沙在泥沙输移过程中容易沉降,而细颗粒泥沙在输移过程中又易于发生絮凝沉降<sup>[24]</sup>,使得过机泥沙粒径的分布区间明显小于土壤颗粒粒径的分布区间。进一步对采集的过机泥沙样品进行级配分析,得知过机泥沙样品在区间 0.3~30 μm 覆盖率均大于 99.5%。

因此,过机泥沙粒径的激光粒度仪测量区间选为 [0.3, 30],按照对数等差递增的方法,将区间划分为 64 个子区间  $I_i = (\varphi_i, \varphi_{i+1})$ ,  $i = 1, 2, 3, \dots, 64$ ,其中  $\lg(\varphi_{i+1}/\varphi_i)$  为一常数。进一步对全部区间进行二进制划分:首先构造一个新的无量纲区间  $J = [\lg(0.3/0.3), \lg(30/0.3)] = [0, 2]$ ,该区间含有 64 个等距子区间  $J_i$ ;再将区间  $J$  依次划分  $N(\epsilon) = 2^k$  个子区间,每个子区间长度  $\epsilon = 2 \times 2^{-k}$ ,为了保证在最小子区间恰好包含测量值,  $k$  的取值范围为 1, 2, 3, 4, 5, 6;最后,  $\mu_i(\epsilon)$  为每个子区间粒径分布的概率密度,利用  $\mu_i(\epsilon)$  构造一个配分函数族<sup>[25]</sup>,有

$$u_i(q, \epsilon) = \frac{\mu_i(\epsilon)^q}{\sum_{i=1}^{N(\epsilon)} \mu_i(\epsilon)^q} \quad (1)$$

粒径分布多重分形的广义维数谱<sup>[26]</sup>为

$$D(q) = \frac{1}{q-1} \lim_{\epsilon \rightarrow 0} \frac{\lg \left[ \sum_{i=1}^{N(\epsilon)} \mu_i(\epsilon)^q \right]}{\lg \epsilon} \quad (q \neq 1) \quad (2)$$

$$D(q) = \lim_{\epsilon \rightarrow 0} \frac{\sum_{i=1}^{N(\epsilon)} \mu_i(\epsilon) \lg \mu_i(\epsilon)}{\lg \epsilon} \quad (q = 1) \quad (3)$$

粒径分布的多重分形奇异性指数为

$$\alpha(q) = \lim_{\epsilon \rightarrow 0} \frac{\sum_{i=1}^{N(\epsilon)} u_i(q, \epsilon) \lg \mu_i(\epsilon)}{\lg \epsilon} \quad (4)$$

相对于奇异性指数的多重分形谱函数为

$$f(q) = \lim_{\epsilon \rightarrow 0} \frac{\sum_{i=1}^{N(\epsilon)} u_i(q, \epsilon) \lg u_i(q, \epsilon)}{\lg \epsilon} \quad (5)$$

式中: $q$ 为从不同层次上提取系统的参量,且取整数。

通过最小二乘法拟合计算,可以分别得到 $D(q)$ 、 $\alpha(q)$ 和 $f(q)$ 。其中,广义维数谱 $D(q)$ 是在不同程度上扫描概率 $\mu_i(\in)$ 的最大子集和最小子集<sup>[27]</sup>。结合公式(2)和(3):当 $q=0$ 时, $D_0$ 中的 $\mu_i(\in)^0$ 均为1,与物理量的概率不均匀分布无关, $D_0$ 反映的是研究对象空间几何性质的均匀度<sup>[27]</sup>;当 $q=1$ 时, $D_1$ 表征了粒径分布整体平均上的不均匀水平<sup>[27]</sup>;当 $q=-1$ 时, $\mu_i(\in)$ 中分子与分母调换,放大的最小子集概率贡献明显大于最大子集概率贡献,提高了最小子集分布的不均匀性分辨率;当 $q=2$ 时, $D_2$ 是在一定程度上放大了最大子集和最小子集概率,但最大子集放大的尺度要明显大于最小子集的尺度,提高了粒径分布测量中最大子集的不均匀分辨率;当 $q=-2$ 时,相较于 $D_{-1}$ , $D_{-2}$ 进一步的提高了粒径分布测量中最小子集的不均匀分辨率,当 $q$ 的绝对值越大,这种相对分辨率越高。多重分形奇异谱谱 $\alpha(q) \sim f(q)$ 能够表述粒径分布的局部特征。其中,多重分形谱的参数 $\alpha_{\max}$ , $f(\alpha_{\max})$ 反映的是粒径分布最小子集的性质, $\alpha_{\min}$ , $f(\alpha_{\min})$ 反映的是粒径分布最大子集的性质,多重分形谱的谱宽 $\Delta\alpha(\alpha_{\max} - \alpha_{\min})$ 反映了粒径分布的不均匀程度, $\Delta\alpha$ 越大表示粒径分布越不均匀<sup>[27]</sup>。

## 2 结果分析

### 2.1 广义维数谱特征分析

令配分函数 $x = \sum_{i=1}^{N(\in)} \mu_i(\in)^q$ ,采用最小二乘法拟合不同 $q$ 值下 $\lg x$ 与 $\lg \in$ 是否呈线性。Meneveau等<sup>[28]</sup>指出, $\lg x$ 与 $\lg \in$ 呈线性是确定研究对象具有分形特征的关键指标, $\lg x$ 与 $\lg \in$ 拟合的线性斜率随 $q$ 的不同取值不变时,研究对象属于单一分形, $\lg x$ 与 $\lg \in$ 拟合的线性斜率随 $q$ 的不同取值不断变化时,研究对象具有多重分形的特征。图1分别为不同过机泥沙样本的配分函数 $x$ 与尺度因子 $\in$ 的双对数拟合图,从图1可以看出当 $q$ 由-10向10以不同程度扫描样品的概率区域,其配分函数 $X$ 和尺度因子 $\in$ 呈现出极显著的线性关系,且线性拟合的斜率随 $q$ 的增大不断递增,其 $R^2$ 均大于0.99。这说明研究区域的过机泥沙具备多重分形特征,可以进行多重分形分析。

采用公式(2)和(3)计算不同过机泥沙样品的广义维数谱。选择 $D_0$ 、 $D_1$ 、 $D_2$ 、 $D_{-1}$ 和 $D_{-2}$ 来作为过机泥沙粒径分布特征的指标,其中, $D_0$ 反映的是研究对象的空间几何性质的均匀度, $D_1$ 表征了粒径分

布整体平均上的不均匀水平, $D_2$ 表征粒径最大子集分布的不均匀性, $D_{-1}$ 和 $D_{-2}$ 是不同程度的反映粒径最小子集分布的不均匀性,见图2。选取研究对象的8个样品进行分析,从图2可以看到,随着 $q$ 值的增加, $D_q$ 表示为反“S”型递减曲线,其中:当 $q=0$ 时,过机泥沙样品的空间区域分布一致,均为对数均匀分布,故八种样品的 $D_0$ 均为1;当 $q=1$ 时,不同过机泥沙样品粒径整体平均分布的不均匀大小为 $D_1(B_2) > D_1(C_1) > D_1(C_2) > D_1(A_2) > D_1(B_1) > D_1(A_1) > D_1(D_2) > D_1(D_1)$ , $D_1$ 越小,分布越不均匀;当 $q=2$ 时,不同过机泥沙样品最大子集粒径不均匀分布大小为 $D_2(B_2) > D_2(B_1) > D_2(C_2) > D_2(C_1) > D_2(A_2) > D_2(A_1) > D_2(D_2) > D_2(D_1)$ ( $D_2$ 越小,分布越不均匀);当 $q=-1$ 时,不同过机泥沙样品最小子集粒径分布的不均匀大小为 $D_{-1}(C_1) > D_{-1}(B_2) > D_{-1}(C_2) > D_{-1}(A_1) > D_{-1}(A_2) > D_{-1}(B_1) > D_{-1}(D_2) > D_{-1}(D_1)$ ;当 $q=-2$ 时,进一步提高了最小子集的不均匀分布分辨率,不同过机泥沙样品粒径分布不均匀大小为 $D_{-2}(C_1) > D_{-2}(B_2) > D_{-2}(C_2) > D_{-2}(A_1) > D_{-2}(A_2) > D_{-2}(D_2) > D_{-2}(B_1) > D_{-2}(D_1)$ 。

当 $q=1$ 时和 $q=2$ 时或当 $q=-1$ 时和 $q=-2$ 时,不同过机泥沙样品最大子集或最小子集的不均匀分布大小有部分差异,主要是因为广义维数谱随着 $q$ 的绝对值不断增加,在不断提高最大子集或最小子集的不均匀分布分辨率大小,而在 $q$ 值较小时,介于最大子集和最小子集的中间区域的概率分布对过机泥沙样品的不均匀分布有较大影响,使得分辨率有待进一步的提高。当 $q$ 的绝对值不断增加时,这种影响不断缩小,而当 $q$ 的绝对值增大达到某一临界值以后,不同过机泥沙样品的不均匀分布大小排名不变。对于最大子集,当 $q \geq 5$ 以后,不同过机泥沙样品粒径分布的不均匀大小为 $D_{\geq 5}(B_2) > D_{\geq 5}(B_1) > D_{\geq 5}(D_2) > D_{\geq 5}(C_2) > D_{\geq 5}(A_2) > D_{\geq 5}(C_1) > D_{\geq 5}(A_1) > D_{\geq 5}(D_1)$ ;对于最小子集,当 $q \leq -7$ 以后,不同过机泥沙样品粒径分布的不均匀大小为 $D_{\leq -7}(C_1) > D_{\leq -7}(B_2) > D_{\leq -7}(A_1) > D_{\leq -7}(D_1) > D_{\leq -7}(C_2) > D_{\leq -7}(D_2) > D_{\leq -7}(A_2) > D_{\leq -7}(B_1)$ 。综上所述,粒径分布整体平均上的不均匀大小为 $D_1(B_2) > D_1(C_1) > D_1(C_2) > D_1(A_2) > D_1(B_1) > D_1(A_1) > D_1(D_2) > D_1(D_1)$ ,最大子集粒径分布的不均匀大小为 $D_{\geq 5}(B_2) > D_{\geq 5}(B_1) > D_{\geq 5}(D_2) > D_{\geq 5}(C_2) > D_{\geq 5}(A_2) > D_{\geq 5}(C_1) > D_{\geq 5}(A_1) > D_{\geq 5}(D_1)$ ;最小子集粒径分布的不均匀大小为 $D_{\leq -7}(C_1) > D_{\leq -7}(B_2) > D_{\leq -7}(A_1) > D_{\leq -7}(D_1) > D_{\leq -7}(C_2) > D_{\leq -7}(A_2) > D_{\leq -7}(D_2) > D_{\leq -7}(B_1)$ 。

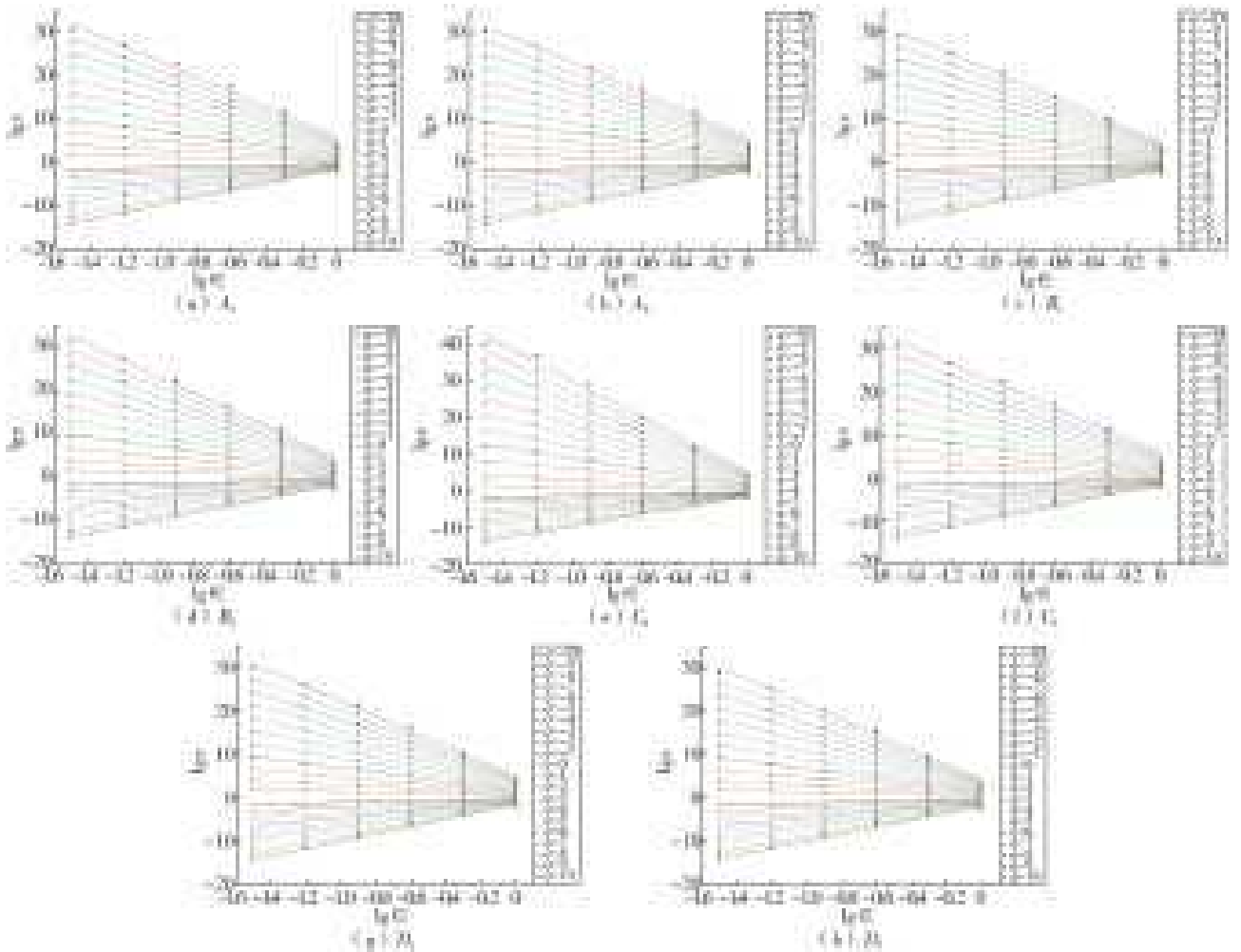


图 1 不同过机泥沙样品配分函数  $\lg x$  与  $\lg \epsilon$  线性拟合

Fig. 1 Linear fitting of the partition function  $\lg x$  and  $\lg \epsilon$  of different machine sediment samples

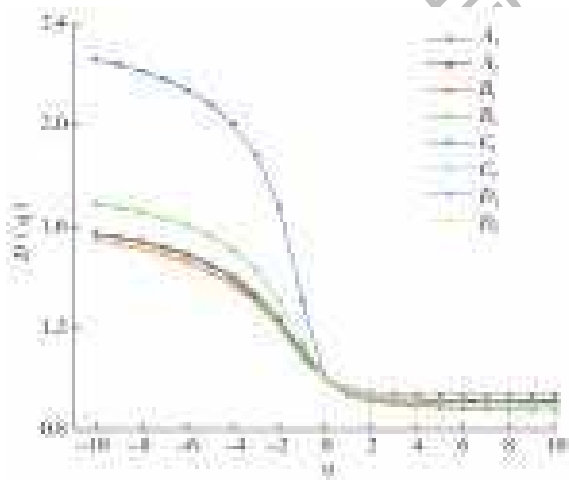


图 2 不同过机泥沙样品广义维数谱  $D(q)-q$  曲线

Fig. 2 Generalized dimensional spectrum  $D(q)-q$  curve of different sediment samples

大小反映了整个分形结构上概率测度分布的非均匀程度,而真正反映概率测度分布整体平均上的不均匀程度的是  $D_1$ 。事实上,多重分形奇异谱谱宽  $\Delta\alpha(=\alpha_{\max}-\alpha_{\min})$  反应的是最大子集和最小子集在  $q=10$  和  $q=-10$  上非均匀程度的叠加,结合广义维数谱计算公式,最大子集和最小子集分布的非均匀大小无法进行有效的比较,故这种简单的叠加不合理。因此,在分析多重分形奇异谱的非均匀程度时,应该将最大子集和最小子集分布分开比较。其中,最小子集的多重分形奇异谱谱宽为  $\Delta\alpha_1(=\alpha_{\max}-\alpha_0)$ ,最大子集的多重分形奇异谱谱宽为  $\Delta\alpha_2(=\alpha_0-\alpha_{\min})$ 。从图 3 可以看到:最小子集粒径分布的不均匀大小为  $\Delta\alpha_1(C_1) > \Delta\alpha_1(B_2) > \Delta\alpha_1(A_1) > \Delta\alpha_1(D_1) > \Delta\alpha_1(C_2) > \Delta\alpha_1(A_2) > \Delta\alpha_1(D_2) > \Delta\alpha_1(B_1)$ ; 最大子集粒径分布的不均匀大小为  $\Delta\alpha_2(B_2) > \Delta\alpha_2(B_1) > \Delta\alpha_2(D_2) > \Delta\alpha_2(C_2) > \Delta\alpha_2(A_2) > \Delta\alpha_2(C_1) > \Delta\alpha_2(A_1) > \Delta\alpha_2(D_1)$ 。结合广义维数谱和多重分形奇异谱,可以看出关于粒径分布在局部上的不均匀程度,两者的结论是相同的,事实上,  $\Delta\alpha_1$

## 2.2 多重分形奇异谱分析

采用公式(4)和(5)计算过机泥沙粒径分布的多重分形奇异谱,见图 3。根据多重分形理论,广义维数谱与多重分形奇异谱是相关联的。大多数文献<sup>[20,29-31]</sup>指出多重分形奇异谱谱宽  $\Delta\alpha(=\alpha_{\max}-\alpha_{\min})$  的

和  $\Delta\alpha_2$  分别反映的是  $q=-10$  和  $q=10$  时,最小子集和最大子集粒径分布的不均匀程度。

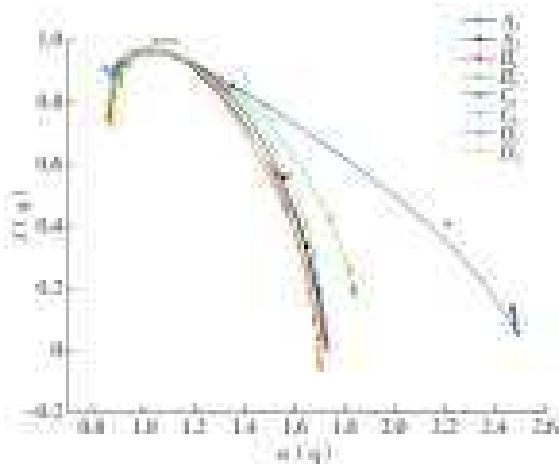


图3 不同过机泥沙样品粒径分布的  $f(q)-\alpha(q)$  曲线  
Fig. 3  $f(q)-\alpha(q)$  curve of particle size distribution of different sediment samples

### 2.3 多重分形参数影响分析

在汛期(6—9月)受降雨侵蚀作用下,存在着水沙峰度,而在水沙二相流中,受上游来流量的影响,使得水沙二相流在加速过程中,受到惯性力的影响,泥沙密度大水流密度小,产生水沙峰度的错开,泥沙含量的峰值比入库流量的峰值要滞后,使得采用入库流量和泥沙质量浓度因素来分析过机泥沙粒径分布的多重分形参数不合理。同样地,过机泥沙的黏粒含量和粉粒含量的跨区域太大,适合分析与单重分形维数的关系,而无法研究多重分形的局部不均匀程度。为此,选择受降雨侵蚀作用下泥沙细化特征参数(中值粒径)来分析多重分形参数的特征。

结合表1中的过机泥沙粒径的多重分形参数和中值粒径,采用最小二乘法分别拟合  $D_{10}$ 、 $D_{-10}$ 、 $\Delta\alpha_1$ 、 $\Delta\alpha_2$  与过机泥沙中值粒径的相关性,见表1、图4至图7。

表1 过机泥沙粒径的多重分形参数

Tab. 1 Multifractal parameters of sediment particle size passing through turbine

过机泥沙样品	$A_1$	$A_2$	$B_1$	$B_2$	$C_1$	$C_2$	$D_1$	$D_2$
$D_0$	1.000 0	1.000 0	1.000 0	1.000 0	1.000 0	1.000 0	1.000 0	1.000 0
$D_1$	0.950 8	0.949 7	0.949 8	0.940 5	0.942 8	0.946 8	0.966 9	0.955 4
$D_2$	0.931 5	0.926 8	0.922 4	0.913 4	0.924 9	0.924 4	0.951 7	0.933 0
$D_{10}$	0.916 8	0.905 6	0.878 9	0.878 6	0.913 5	0.904 7	0.940 1	0.893 4
$D_{-1}$	1.114 8	1.105 8	1.095 0	1.141 4	1.310 2	1.117 7	1.081 4	1.094 1
$D_{-2}$	1.245 2	1.228 0	1.207 6	1.309 3	1.679 0	1.247 4	1.204 7	1.211 4
$D_{10}$	1.577 3	1.571 5	1.549 0	1.690 6	2.261 1	1.572 4	1.576 3	1.553 0
$\Delta\alpha_1$	0.681 3	0.646 9	0.637 8	0.743 6	1.348 6	0.647 5	0.648 1	0.638 1
$\Delta\alpha_2$	0.216 4	0.191 5	0.167 4	0.165 5	0.206 8	0.184 9	0.225 8	0.176 2
中值粒径	0.002 0	0.002 0	0.002 3	0.002 2	0.002 0	0.002 1	0.001 8	0.002 2

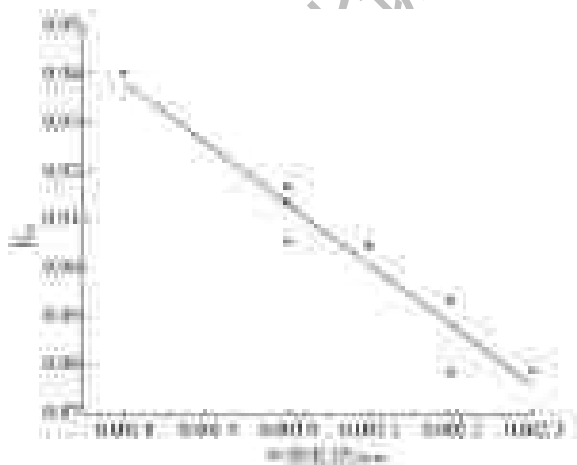


图4 过机泥沙粒径  $D_{10}$  与中值粒径的关系  
Fig. 4 Relationship between particle size  $D_{10}$  and median particle size

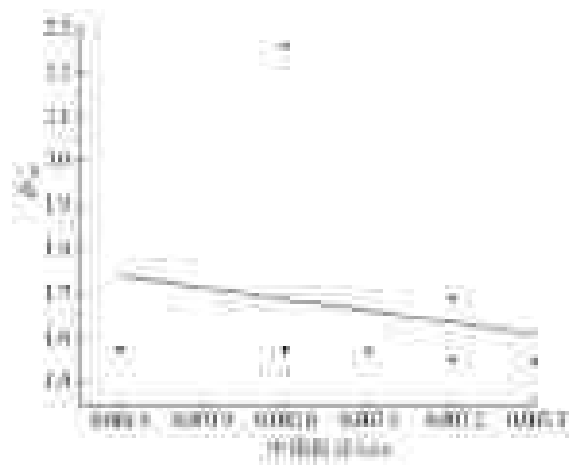


图5 过机泥沙粒径  $D_{-10}$  与中值粒径的关系  
Fig. 5 Relationship between particle size  $D_{-10}$  and median particle size

选择相关决定系数  $R^2$  来作为判别相关性的依据,其中  $R^2$  在区间范围  $[0, 0.091 6]$  为无弱相关性,在  $(0.091 6, 0.304 9]$  为弱中等相关性,在  $(0.304 9, 0.508 1]$  为中等相关性,在  $(0.508 1, 1]$  属于强相关

性。图4和5分别为  $D_{10}$ 、 $D_{-10}$  与过机泥沙中值粒径的相关性分析,其中  $D_{10}$ 、 $D_{-10}$  与过机泥沙中值粒径的相关性系数分别为  $R^2=0.92$ 、 $R^2=0.03$ ;图6和7为  $\Delta\alpha_1$ 、 $\Delta\alpha_2$  与过机泥沙中值粒径的相关性分析。其中

$\Delta\alpha_1$ 、 $\Delta\alpha_2$  与过机泥沙中值粒径的相关性系数分别为  $R^2=0.03$ 、 $R^2=0.93$ 。 $D_{10}$ 、 $\Delta\alpha_2$  是表征最大子集不均匀程度的多重分形参数, $D_{-10}$ 、 $\Delta\alpha_1$  是表征最小子集不均匀程度的多重分形参数,过机泥沙中值粒径能够表征泥沙细化程度,通过相关性分析,可以看出泥沙细化和最大子集分布不均匀大小呈现强的负相关性,而泥沙细化和最小子集分布不均匀大小无关。进一步,泥沙细化主要受到泥沙颗粒输移起动规律的影响,具体表现在粗沙在河流输移中容易先沉降不易起动,而细沙则容易发生絮凝沉降,使得泥沙分布区域束窄,最大子集概率增加,增大了最大子集分布的不均匀大小,而对于稀疏区域的影响不明显。

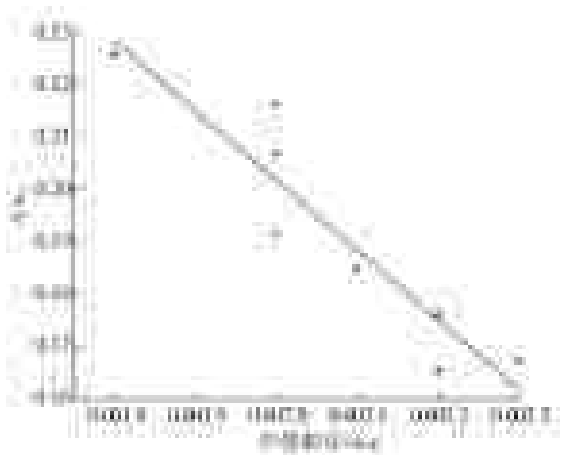


图 6 过机泥沙粒径  $\Delta\alpha_2$  与中值粒径的关系

Fig. 6 Relationship between particle size  $\Delta\alpha_2$  and median particle size

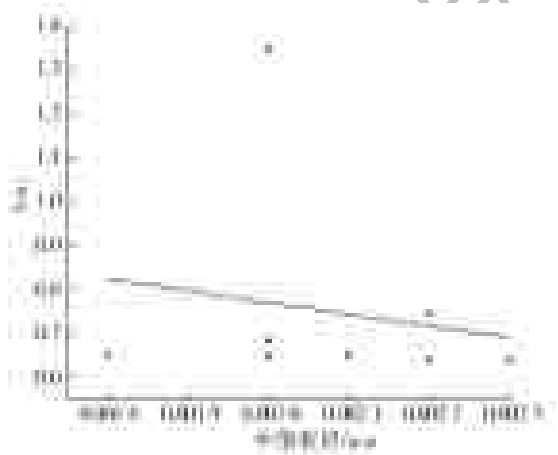


图 7 过机泥沙粒径  $\Delta\alpha_1$  与中值粒径的关系

Fig. 7 Relationship between particle size  $\Delta\alpha_1$  and median particle size

### 3 结 论

本文探索过机泥沙粒径的分布特征规律能为防护水轮机过流部件提供理论支撑和技术参考。以向家坝水电站过机泥沙为研究对象,采用激光粒度仪分析过机泥沙粒径级配的体积百分比,运用多重分

形理论对粒径分布的特征规律进行研究,研究结果如下。

(1)结合广义维数谱:当  $q \geq 2$  时, $D_{q \geq 2}$  反映的是最大子集分布的不均匀性,且  $q$  越大,最大子集分布的不均匀性分辨率越高;当  $q \leq -1$  时, $D_{q \leq -1}$  反映的是最小子集分布的不均匀性,且  $q$  越小,最小子集分布的不均匀性分辨率越高。

(2)向家坝水电站过机泥沙粒径分布整体平均上的不均匀大小为  $D_1(B_2) > D_1(C_1) > D_1(C_2) > D_1(A_2) > D_1(B_1) > D_1(A_1) > D_1(D_2) > D_1(D_1)$ ; 存在某一阈值,使得当  $q \geq 5$ ,最大子集粒径分布的不均匀大小为  $D_{\geq 5}(B_2) > D_{\geq 5}(B_1) > D_{\geq 5}(D_2) > D_{\geq 5}(C_2) > D_{\geq 5}(A_2) > D_{\geq 5}(C_1) > D_{\geq 5}(A_1) > D_{\geq 5}(D_1)$ ; 当  $q \leq -7$  时,最小子集粒径分布的不均匀大小为  $D_{\leq -7}(C_1) > D_{\leq -7}(B_2) > D_{\leq -7}(A_1) > D_{\leq -7}(D_1) > D_{\leq -7}(C_2) > D_{\leq -7}(A_2) > D_{\leq -7}(D_2) > D_{\leq -7}(B_1)$ 。

(3)结合广义维数谱,向家坝水电站过机泥沙粒径最大子集和最小子集分布的非均匀大小无法进行有效的比较,结合多重分形奇异谱谱宽为  $\Delta\alpha_1$  和  $\Delta\alpha_2$ ,最大子集粒径分布的不均匀大小为  $\Delta\alpha_1(B_2) > \Delta\alpha_1(B_1) > \Delta\alpha_1(D_2) > \Delta\alpha_1(C_2) > \Delta\alpha_1(A_2) > \Delta\alpha_1(C_1) > \Delta\alpha_1(A_1) > \Delta\alpha_1(D_1)$ ,最小子集粒径分布的不均匀大小为  $\Delta\alpha_2(C_1) > \Delta\alpha_2(B_2) > \Delta\alpha_2(A_1) > \Delta\alpha_2(D_1) > \Delta\alpha_2(C_2) > \Delta\alpha_2(A_2) > \Delta\alpha_2(D_2) > \Delta\alpha_2(B_1)$ 。

(4)结合相关性分析,泥沙细化和最大子集分布不均匀大小呈现良好的负相关性,而泥沙细化和最小子集分布不均匀大小无关。

#### 参考文献(References):

- [1] 张瑞瑾. 河流泥沙动力学[M]. 北京:中国水利水电出版社,1998. (ZHANG R J. Dynamics of river sediments [M]. Beijing: China Water Resources and Hydropower Press, 1998. (in Chinese)) DOI: 10. 1002/(SICI)1096-9837(199702)22:2<192::AID-ESP650>3. 0. CO;2-2.
- [2] MORGAN R P C. Soil erosion and conservation[J]. Earth Science Reviews, 1985, 24 (1): 68-69. DOI: 10. 1002/(SICI)1096-9837(199702)22:2<192::AID-ESP650>3. 0. CO;2-2.
- [3] GUI D, LEI J, ZENG F, et al. Characterizing variations in soil particle size distribution in oasis farmlands: A case study of the Cele Oasis[J]. Mathematical & Computer Modelling, 2010, 51(1112): 1306-1311. DOI: 10. 1016/j. mcm. 2009. 10. 035.
- [4] OLESCHKO K, B FIGUEROA S, MIRANDA M E, et al. Mass fractal dimensions and some selected physical properties of contrasting soils and sediments of Mexico

- [J]. *Soil & Tillage Research*, 2000, 55(1): 43-61. DOI: 10.1016/S0167-1987(00)00097-0.
- [5] 李占海, 陈沈良, 高抒, 等. 长江口南支边滩悬沙级配的现场与室内观测结果的比较分析[J]. *泥沙研究*, 2010(1): 37-45. (LI Z H, CHEN S L, GAO S, et al. Comparative analysis of on-site and indoor observation results of suspended sand grading in the southern branch of the Yangtze River estuary[J]. *Journal of Sediment Research*, 2010(1): 37-45. (in Chinese)) DOI: 10.16239/j.cnki.0468-155x.2010.01.005.
- [6] 王党伟, 吉祖稳, 邓安军, 等. 絮凝对三峡水库泥沙沉降的影响[J]. *水利学报*, 2016, 47(11): 1389-1396. (WANG D W, JI Z W, DENG A J, et al. Influence of flocculation on sediment deposition in the Three Gorges Reservoir[J]. *Journal of Hydraulic Engineering*, 2016, 47(11): 1389-1396. (in Chinese)) DOI: 10.13243/j.cnki.slxb.20160058.
- [7] 宋玉亮, 郭成久, 范昊明, 等. 大凌河中下游泥沙颗粒特征分析[J]. *人民黄河*, 2010, 32(2): 42-43. (SONG Y L, GUO C J, FAN H M, et al. Characteristics analysis of sediment particles in the middle and lower reaches of Daling River[J]. *Yellow River*, 2010, 32(2): 42-43. (in Chinese)) DOI: 10.3969/j.issn.1000-1379.2010.02.019.
- [8] 王金花, 张荣刚, 姚文艺, 等. 风蚀水蚀共同作用下沙漠河流泥沙级配特征[J]. *中国沙漠*, 2016, 36(6): 1695-1700. (WANG J H, ZHANG R G, YAO W Y, et al. Sediment grading characteristics of desert rivers under the combined action of wind erosion and water erosion[J]. *Journal of Desert Research*, 2016, 36(6): 1695-1700. (in Chinese)) DOI: 10.7522/j.issn.1000-694x.2016.00181.
- [9] 肖毅, 王虹, 邵学军, 等. 考虑泥沙分选及床沙级配调整的二维数值模拟研究[J]. *工程科学与技术*, 2012(s1): 60-65. (XIAO Y, WANG H, SHAO X J, et al. Two-dimensional numerical simulation of sediment separation and bed sand grading adjustment[J]. *Engineering Science and Technology*, 2012(s1): 60-65. (in Chinese)) DOI: 10.15961/j.jsuese.2012.s1.017.
- [10] 张广, 魏显著. 泥沙浓度及粒径对水轮机转轮内部流动影响的数值分析[J]. *农业工程学报*, 2014, 30(23): 94-100. (ZHANG G, WEI X Z. Numerical analysis of the influence of sediment concentration and particle size on the internal flow of turbine runner[J]. *Transactions of the Chinese Society of Agricultural Engineering*, 2014, 30(23): 94-100. (in Chinese)) DOI: 10.3969/j.issn.1002-6819.2014.23.013.
- [11] 黄廷杰, 陆彦, 陈帅, 等. 床沙粒径及级配非均匀沙起动的非均匀沙起动的分析[J]. *人民黄河*, 2015, 37(1): 34-37. (HUANG T J, LU Y, CHEN S, et al. Analysis of the influence of particle size and grade on the start of non-uniform sand[J]. *Yellow River*, 2015, 37(1): 34-37. (in Chinese)) DOI: 10.3969/j.issn.1000-1379.2015.01.009.
- [12] 任岩. 泥沙粒径级配对水轮机材料磨蚀性能的影响[J]. *水力发电*, 2011, 37(8): 62-63. (REN Y. Influence of sediment particle size on the abrasive properties of turbine materials[J]. *Hydroelectric Power*, 2011, 37(8): 62-63. (in Chinese))
- [13] MANDELROT B, YORK N, BASSINGTHWAITE J, et al. *The Fractal Geometry of Nature* [M]. New York: W. H. Freeman, 1983: 468.
- [14] PERFECT E, KAY B D. Applications of fractals in soil and tillage research: A review[J]. *Soil & Tillage Research*, 1995, 36(1/2): 1-20. DOI: 10.1016/0167-1987(96)81397-3.
- [15] MAGGI F, MIETTA F, WINTERWERP J C. Effect of variable fractal dimension on the floc size distribution of suspended cohesive sediment[J]. *Journal of Hydrology*, 2007, 343(1): 43-55. DOI: 10.1016/j.jhydrol.2007.05.035.
- [16] 杨帅, 李永红, 高照良, 等. 黄土堆积体植物篱减沙效益与泥沙颗粒分形特征研究[J]. *农业机械学报*, 2017, 48(8): 270-278. (YANG S, LI Y H, GAO Z L, et al. Study on the benefits of sediment reduction and the fractal characteristics of sediment particles in loess accumulation[J]. *Transactions of the Chinese Society of Agricultural Machinery*, 2017, 48(8): 270-278. (in Chinese)) DOI: 10.6041/j.issn.1000-1298.2017.08.031.
- [17] 刘森, 吴媛媛, 杨明义, 等. 次降雨过程中侵蚀泥沙分形维数的变化特征[J]. *中国水土保持科学*, 2015, 13(2): 37-43. (LIU M, WU Y Y, YANG M Y, et al. Variation characteristics of erosion and sediment fractal dimension during sub-rainfall[J]. *Chinese Journal of Soil and Water Conservation*, 2015, 13(2): 37-43. (in Chinese)) DOI: 10.16843/j.sswc.2015.02.006.
- [18] GROUT H, TARQUIS A M, WIESNER M R. Multi-fractal analysis of particle size distributions in soil[J]. *Environmental Science & Technology*, 1998, 32(32): 1176-1182.
- [19] WANG D, FU B, ZHAO W, et al. Multifractal characteristics of soil particle size distribution under different land-use types on the Loess Plateau, China[J]. *Catena*, 2008, 72(1): 29-36. DOI: 10.1016/j.catena.2007.03.019.
- [20] 白一茹, 汪有科. 黄土丘陵区土壤粒径分布多重分形和多重分形特征[J]. *农业机械学报*, 2012, 43(5): 43-48. (BAI Y R, WANG Y K. Single fractal and multifractal characteristics of soil particle size distribution in Loess Hilly Region[J]. *Transactions of the Chinese Society of Agricultural Machinery*, 2012, 43(5): 43-48. (in Chinese)) DOI: 10.6041/j.issn.1000-1298.2012.05.008.
- [21] 管孝艳, 杨培岭, 任树梅, 等. 基于多重分形理论的壤土粒径分布非均匀性分析[J]. *应用基础与工程科学学报*, 2009, 17(2): 196-205. (GUAN X Y, YANG P

- L, REN S M, et al. Non-uniformity analysis of loam particle size distribution based on multifractal theory [J]. *Journal of Basic Science and Engineering*, 2009, 17(2): 196-205. (in Chinese) DOI: 10. 16058/j. issn. 1005-0930. 2009. 02. 014.
- [22] 王剑. 降雨驱动下侵蚀泥沙颗粒分选特征及搬运机制 [D]. 武汉: 华中农业大学, 2015. (WANG J. Separation characteristics and handling mechanism of eroded sediment particles driven by rainfall [D]. Wuhan: Huazhong Agricultural University, 2015. (in Chinese))
- [23] 韩其为. 泥沙起动规律及起动流速 [J]. *泥沙研究*, 1982(2): 13-28. (HAN Q W. The law of sediment initiation and starting velocity [J]. *Sediment Research*, 1982(2): 13-28. ) DOI: 10. 16239/j. cnki. 0468-155x. 1982. 02. 002.
- [24] 柴朝晖, 李昊洁, 王茜, 等. 黏性泥沙絮凝研究进展 [J]. *长江科学院院报*, 2016, 33(2): 1-9. (CHAI Z H, LI H J, WANG Q, et al. Research progress of cohesive sediment flocculation [J]. *Journal of Yangtze River Scientific Research Institute*, 2016, 33(2): 1-9. (in Chinese) DOI: 10. 11988/ckyyb. 20140855.
- [25] 周炜星, 吴韬, 于遵宏. 多重分形奇异谱的几何特性 II. 配分函数法 [J]. *华东理工大学学报*, 2000, 26(4): 390-395. (ZHOU W X, W T, YU Z H. Geometrical properties of multifractal singular spectrum II. partition function method [J]. *Journal of East China University of Science and Technology*, 2000, 26(4): 390-395. (in Chinese) DOI: 10. 14135/j. cnki. 1006-3080. 2000. 04. 018.
- [26] ZELEKE T B, SI B C. Scaling relationships between saturated hydraulic conductivity and soil physical properties [J]. *Soil Science Society of America Journal*, 2005, 69 (6): 1691-1702. DOI: 10. 2136/SS-SAJ2005. 0072.
- [27] 孙洪泉. 分形几何与分形插值 [M]. 北京: 科学出版社, 2011. (SUN H Q. *Fractal Geometry and Fractal Interpolation* [M]. Beijing: Science Press, 2011. (in Chinese))
- [28] MENEVEAU C, SREENIVASAN K R, KAILASNATH P, et al. Joint multifractal measures: Theory and applications to turbulence [J]. *Physical Review A*, 1990, 41 (2): 894-913.
- [29] 孙哲, 王一博, 刘国华, 等. 基于多重分形理论的多年冻土区高寒草甸退化过程中土壤粒径分析 [J]. *冰川冻土*, 2015, 37(4): 980-990. (SUN Z, WANG Y B, LIU G H, et al. Analysis of soil particle size during alpine meadow degradation in permafrost regions based on multifractal theory [J]. *Journal of Glaciology and Geocryology*, 2015, 37(4): 980-990. (in Chinese) DOI: 10. 7522/j. issn. 1000-0240. 2015. 0109.
- [30] 管孝艳, 杨培岭, 吕焯. 基于多重分形的土壤粒径分布与土壤物理特性关系 [J]. *农业机械学报*, 2011, 42 (3): 44-50. (GUAN X Y, YANG P L, LYU Y. Relationship between soil particle size distribution and soil physical properties based on multifractal [J]. *Transactions of the Chinese Society of Agricultural Machinery*, 2011, 42(3): 44-50. (in Chinese))
- [31] 黄运湘, 徐明岗, 孙楠, 等. 长期不同施肥红壤粒径分布的多重分形特征 [J]. *中国农业科学*, 2014, 47(11): 2173-2181. (HUANG Y X, XU M G, SUN N, et al. Multifractal characteristics of particle size distribution of long-term fertilization red soil [J]. *Scientia Agricultura Sinica*, 2014, 47(11): 2173-2181. (in Chinese) DOI: 10. 3864/j. issn. 0578-1752. 2014. 11. 011.

### Multifractal characteristics of sediment pass by the Xiangjiaba Hydropower Station

LIU Chaofan<sup>1</sup>, XIA Wei<sup>1</sup>, WANG Jibao<sup>1</sup>, XU Xuewen<sup>2</sup>, CHEN Hechun<sup>1</sup>, CHEN Yanchao<sup>1</sup>

(1. College of Hydraulic and Environmental Engineering, China Three Gorges University, Yichang 443002, China;

2. Hubei provincial water conservancy and hydropower planning survey and design institute, Wuhan 430064, China)

**Abstract:** The power generation efficiency problem and hydropower stations turbine abrasion overwhelmed water conservancy engineers, especially during the flood season, when heavy rains, and the inflow and sediment concentration have reached their peaks. The power generation efficiency of hydropower stations is the best during this period, while the flow components of the turbine are also subject to abrasion. The Xiangjiaba Hydropower Station is located in the lower reaches of the Jinsha River. After its completion, it exerts tremendous flood control and power generation benefits. As the core equipment of the power station, the performance of the hydraulic turbine and the reliability of its operation are some of the keys to whether it can exert engineering benefits. To understand the rules of damage to hydraulic turbines by sediment in time, and to study various protective measures to reduce the abrasion damage to the surface of the turbine's flow-passing parts by the sand-containing water flow, it is necessary to carry out the medium- and long-term monitoring of the sediment of the typical units on the left and right banks of the Xiangjiaba Hydropower Station to provide data support for the subsequent development of hydraulic turbine protection measures.

The Xiangjiaba Hydropower Station flood season from June to September is taken as the research object. The maximum sediment concentration is selected twice a month by taking into account the time difference of the sediment particle size distribution during the flood season. The silt is sampled by the machine. For each sample, the left and right bank typical units are selected and enter the designated water intake inside the turbine volute for water sample collection. A total of 8 samples were taken during the entire flood season. After sampling the laser particle size analyzer was used to analyze the volume percentage of the



machine-silt particle size gradation. The characteristic law of particle size distribution was studied using multifractal analysis.

The results show that the particle size of the machined sediment has good multifractal characteristics. Combined with the multifractal theory, the overall average inhomogeneity of the particle size distribution is  $D_1(B_2) > D_1(C_1) > D_1(C_2) > D_1(A_2) > D_1(B_1) > D_1(A_1) > D_1(D_2) > D_1(D_1)$ . There is a certain threshold, so that when, the uneven size of the largest subset particle size distribution is  $D_{\geq 5}(B_2) > D_{\geq 5}(B_1) > D_{\geq 5}(D_2) > D_{\geq 5}(C_2) > D_{\geq 5}(A_2) > D_{\geq 5}(C_1) > D_{\geq 5}(A_1) > D_{\geq 5}(D_1)$ , at that time, the uneven size of the smallest subset particle size distribution is  $D_{\leq -7}, D_{\leq -7}(C_1) > D_{\leq -7}(B_2) > D_{\leq -7}(A_1) > D_{\leq -7}(D_1) > D_{\leq -7}(C_2) > D_{\leq -7}(A_2) > D_{\leq -7}(D_2) > D_{\leq -7}(B_1)$  ( $A_1, B_1, C_1, D_1$  are the sediment sample numbers of the left bank unit, and  $A_2, B_2, C_2, D_2$  is the sediment sample number of the right bank unit). Combined with the generalized dimensional spectrum, the non-uniform distribution of the largest subset and the smallest subset of the sediment size of the Xiangjiaba Hydropower Station can not be effectively compared. Combined with the multifractal singularity, the spectrum width is  $\Delta\alpha_1$  and  $\Delta\alpha_2$ , and the uneven size of the largest subset particle size distribution is  $\Delta\alpha_1(B_2) > \Delta\alpha_1(B_1) > \Delta\alpha_1(D_2) > \Delta\alpha_1(C_2) > \Delta\alpha_1(A_2) > \Delta\alpha_1(C_1) > \Delta\alpha_1(A_1) > \Delta\alpha_1(D_1)$ . The smallest subset particle size distribution is  $\Delta\alpha_2(C_1) > \Delta\alpha_2(B_2) > \Delta\alpha_2(A_1) > \Delta\alpha_2(D_1) > \Delta\alpha_2(C_2) > \Delta\alpha_2(A_2) > \Delta\alpha_2(D_2) > \Delta\alpha_2(B_1)$ .

Combining the generalized dimensional spectrum and the multifractal singular spectrum, the two conclusions are the same regarding the local unevenness of the particle size distribution. Combined with the correlation analysis, the sediment refinement and the maximum subset distribution unevenness show good results. The negative correlation of the silt refinement has nothing to do with the uneven size of the smallest subset distribution.

**Key words:** hydropower station; overburden sediment; multifractal theory; particle size distribution

(上接第 571 页)

The results show that: (1) Surface water has low mineralization and is weakly alkaline, and the water chemistry type is mainly  $\text{HCO}_3 \cdot \text{SO}_4 \cdot \text{Cl-Ca}$  type water. The overall mineralization of groundwater is low and weakly alkaline, and the water chemistry type is mainly  $\text{HCO}_3\text{-Na} \cdot \text{Ca}$  type,  $\text{Cl-Na}$  type,  $\text{HCO}_3 \cdot \text{Ca} \cdot \text{Mg}$  type, and  $\text{HCO}_3 \cdot \text{Cl-Na}$  type water. (2) The average value of  $\delta(D)$  of Yellow River water is  $-79.6\%$ , and the  $\delta(^{18}\text{O})$  is  $-10.7\%$ , respectively. The average value of  $\delta(D)$  of Quaternary water is  $-66.25\%$ , and the  $\delta(^{18}\text{O})$  is  $-9.1\%$ , respectively. The average value of  $\delta(D)$  of Cretaceous water is  $-70.6\%$ , and the  $\delta(^{18}\text{O})$  is  $-9.3\%$ , respectively. The average value of  $\delta(D)$  of Carboniferous-Permian water is  $-77.07\%$ , and the  $\delta(^{18}\text{O})$  is  $-9.9\%$ , respectively. The average value of Cambrian-Ordovician water  $\delta(D)$  average value is  $-75.73\%$ ,  $\delta(^{18}\text{O})$  is  $-10.06\%$ . Atmospheric precipitation is influenced by polar air masses and southeastern monsoons, and the principal sources are westerly water vapor, surface water, and groundwater vapor evaporation recirculation. (3) The fourth system water has high tritium content, the presence of nuclear explosive tritium, and excellent groundwater runoff conditions. The Cretaceous water has low tritium content and is a mixture of groundwater recharged before 1952 and recently recharged water. The Carboniferous-Permian water contains a wide range of tritium content, including groundwater recharged before 1952 and modern water. The Cambrian-Ordovician water contains a wide range of tritium content, including groundwater recharged before 1952, modern water, and mixed water. (4) The recharge ratio of atmospheric precipitation to Cambrian-Australian water ranges from  $0.98\%$  to  $91.7\%$ , with an average recharge rate of  $61.2\%$ . The recharge ratio of surface water (referred to as Yellow River water) to Cambrian-Ordovician water ranges from  $0.83\%$  to  $90.2\%$ , with an average recharge rate of  $38.8\%$ . Among them, the recharge ratio of Yellow River water to Cambrian-Ordovician water is larger in Longwanggou, Suancigou, and Huangyuchuan well field, which is influenced by the development of geological structures.

The fault zone and the fracture zone of the fold axis are the main water-conducting channels between different aquifers. Atmospheric precipitation and the Yellow River are the principal sources of groundwater recharge. The precipitation vapor sources are mainly westerly water vapor, surface water, and groundwater vapor evaporation recirculation. Highly pressurized head Cambrian-Ordovician karst fracture water cross-flow recharges the Fourth Series and sandstone fracture water. The pore water of the Fourth Series recharges the fracture water of the Carboniferous-Permian sandstone downward through the fracture development zone of the unconformity contact surface between the strata. The recharge ratio of the Yellow River to Cambrian-Australian water is influenced by the development of geological structures. In Longwanggou, Suancigou, and Huangyuchuan well field, the proportion of recharge of the Yellow River water to Cambrian-Ordovician water is larger.

**Key words:** groundwater circulation; HYSPPLIT model; stable isotope; groundwater age; replenishment ratio; Jungar coalfield area